International Society for Biofabrication
PURPOSE-LED PUBLISHING™

PAPER • **OPEN ACCESS**

Biomimetic multilayered hydrogel scaffold with dual cell types and mesh support for urethral reconstruction

To cite this article: Aivaras Grybas *et al* 2026 *Biofabrication* **18** 035048

View the article online for updates and enhancements.

You may also like

- Micro-comb 3D printing: rapid fabrication of tissue-guiding substrates using micro-embossed nozzles
Sarkhan Butdayev, Stefan Leone, Shayla Nikzad et al.
- Improved quality and reproducibility of cerebral cortical organoids under microfluidic culture conditions: a proof-of-concept study
Héloïse Castiglione, Lucie Madrange, Nuno Brás et al.
- *In situ* rheological monitoring of diffusion-controlled hydrogel crosslinking for embedded 3D bioprinting
Fotis Christakopoulos, Audrey Shih, Stella J Chung et al.



This content was downloaded from IP address 158.129.162.194 on 12/11/2026 at 12:43

Biofabrication

Check for updates

OPEN ACCESS

RECEIVED
31 October 2025

REVISED
25 June 2026

ACCEPTED FOR PUBLICATION
3 August 2026

PUBLISHED
24 August 2026

Original content from this work may be used under the terms of the Creative Commons Attribution 4.0 licence.

Any further distribution of this work must maintain attribution to the author(s) and the title of the work, journal citation and DOI.

PAPER

Biomimetic multilayered hydrogel scaffold with dual cell types and mesh support for urethral reconstruction

Aivaras Grybas[1], Povilas Barasa[2], Darius Dasevicius[3], Andrius Buivydas[2], Ramune Tamasauske Zilinskaite[4], Emilija Baltrukonyte[2], Ieva Simoliune[2], Milda Alksne[2], Natalija Krestnikova[2], Arunas Zelvys[1], Daiva Baltriukiene[2], Gilvydas Verkauskas[4], Feliksas Jankevicius[1] and Egidijus Simoliunas[2,*]

[1] Vilnius University Hospital Santaros klinikos, Center of Urology, Vilnius, Lithuania
[2] Vilnius University, Life Science Center, Institute of Biochemistry, Vilnius, Lithuania
[3] National Center of Pathology, Affiliate of Vilnius University Hospital Santaros klinikos, Vilnius, Lithuania
[4] Vilnius University, Faculty of Medicine, Institute of Clinical Medicine, Clinic of Gastroenterology, Nephro-Urology and Surgery, Vilnius, Lithuania
[*] Author to whom any correspondence should be addressed.

E-mail: egidijus.simoliunas@gmc.vu.lt

Keywords: bioprinting, urethra reconstruction, stem cells, rabbit

Supplementary material for this article is available online

Abstract

Urethral strictures and hypospadias remain major challenges in urology, with current treatments limited by donor-site morbidity, graft shrinkage, and poor long-term outcomes. To address these limitations, we developed a biomimetic multilayered hydrogel scaffold with dual cell types and mesh reinforcement for urethral reconstruction. The construct combined predifferentiated buccal mucosa cells and adipose-derived mesenchymal stem cells within a gelatin methacrylate-silk fibroin hydrogel supported by electrowritten and electrospun polymeric meshes, designed to reproduce both epithelial and smooth muscle layers of the native urethra. Implanted into the rabbit urethra and followed for 12 weeks, the scaffold showed favorable integration with early but transient immune activation, preservation of systemic stability, and maintenance of urethral lumen architecture. Histological evaluation revealed the formation of a stratified urothelium and organized smooth muscle bundles with limited fibrosis, highlighting the scaffold's potential to support functional urethral regeneration and serve as an alternative to graft-based urethroplasty.

1. Introduction

Urethral strictures remain a serious challenge in contemporary urology and are still common. Hospital episode statistics suggest that urethral strictures affect males with an increasing incidence from about 1 in every 10 000 men aged 25 to about 1 in every 1000 men aged 65 or more [1]. Noteworthily, 40.6% of these patients experience at least one complication directly related to urethral stricture including acute urinary retention (32.6%), difficult catheterization (16.0%), urethral abscess/urosepsis (5.0%), or renal failure (3.1%). Even more, 7.0% of patients experienced complications deemed to be life-threatening [2]. In childhood, the urethra can be affected by a congenital disorder—hypospadia. This is a birth defect in which the urethral opening is not at the tip, but at the base of the penis, even in the scrotum or perineum. It is also a fairly common condition, occurring in about 1 in 467 male births [3]. Hypospadias, if left untreated, can cause urinary, sexual, and psychological complications. In most cases, surgical correction of hypospadias in early childhood is successful, but complications occur in up to 10% of mild cases and up to 50% of severe. Most of these patients develop urethral strictures and require a more complex extended urethroplasty with tissue replacement [4]. Complicated and recurrent urethral strictures require long-term treatment with uncertain final outcomes. These are treated in stages with substitutional urethroplasty using different graft or flap techniques. The most common types of grafts used to repair urethral strictures are taken from the buccal mucosa, preputial skin, skin flaps, or other sources [5]. Unfortunately, these grafts are limited due to tissue shortage, donor site morbidity, transplant shrinkage,

© 2026 The Author(s). Published by IOP Publishing Ltd

and scarring. This is especially true for strictures of greater length, severe spongiosclerosis, lichen sclerosus, and cases of failed treatment of hypospadias [6, 7].

The randomized study compared the buccal mucosa graft (BMG) and penile skin flap urethroplasty [8]. The results reported significantly higher operative time in the penile skin flap group (mean 224 min) compared to BMG group (162 min, $p = 0.001$). 32% patients (9 of 28) had postoperative complications in the penile skin flap group: 6 patients had superficial penile skin necrosis, 1 had extensive skin loss and required skin grafting, and 2 had penile torsion. In the BMG group 25.6% of patients had minor morbidity which settled by 4 weeks after surgery, including perioral numbness (4/27), increased salivation (3/27), wound infection (1/27), post-void dribbling (4/27). Final success rate after mean folowup of 22.6 and 24.2 months respectively, in the BMG group reached 89.9% and penile skin flap group—85.6% ($p > 0.05$).

Tissue engineering could be a promising option for advanced substitutional urethroplasties. In the context of urethral biofabrication, several scaffold concepts have been explored, ranging from decellularized matrices and acellular synthetic scaffolds to cell-seeded hydrogels and multilayered constructs. Acellular scaffolds are easier to manufacture and provide a structural template, but their regenerative outcome depends largely on host cell infiltration and remodeling, which may be delayed or accompanied by inflammation and fibrosis. Naturally sourced acellular grafts, such as urinary bladder matrice (UBM) or small intestinal submucosa (SIS) where recently well studied in the animal studies as well as in clinical trials on humans [9, 10].

A randomized clinical trial of 30 patients compared acellular UBM with BMG. The study showed that a stable urethral patency was maintained after the procedure in 66.6% and 100% of cases, respectively [11]. In Palminteri *et al* study 25 men (mean age 40.5 years) with bulbar strictures underwent patch graft urethroplasty using SIS placed on the dorsal or ventral or dorsal plus ventral surface of the urethra [12]. The mean follow-up period was 71 months. Final results revealed 19 (76%) were successful and 6 (24%) were failures. SIS grafts showed similar results to penile skin grafts but were less effective than BMG.

According available data, neither the American Urological Association (AUA) nor the European Association of Urology recommends SIS or other synthetic/animal allografts for standard urethroplasty. The guidelines indicate that these materials tend to yield poorer results compared to BMG, particularly when the local urethral bed is unhealthy or scarred. They note that cell-free matrices used alone without autologous cell seeding are not ideal for full-thickness urethral reconstruction. The AUA specifically states that surgeons should not perform substitution urethroplasty with allograft, xenograft, or synthetic materials (such as SIS) except under experimental protocols. They designate oral mucosa as the first choice when a graft is needed [13].

Cell-seeded scaffolds can provide a more biologically active microenvironment by introducing epithelial, stromal, or smooth muscle-like cells before implantation; however, their fabrication requires reproducible protocols that preserve cell viability while providing sufficient handling strength for surgery. Gelatin methacrylate (GelMA)-based hydrogels are attractive for this purpose because they are photocrosslinkable, cell-compatible, and suitable for extrusion-based bioprinting, while silk fibroin can improve hydrogel cohesion and mechanical handling. Nevertheless, hydrogel-only constructs often remain too fragile for suturing and implantation, making reinforcement with electrospun or electrowritten polymeric meshes a practical strategy to improve surgical applicability without losing the biological advantages of the hydrogel phase [9, 14, 15].

Alternatively, mesenchymal stem cells, known for their anti-inflammatory properties, can be isolated from the patient's oral cavity or adipose tissue [16]. Nevertheless, this poses additional challenges, as undifferentiated stem cells can migrate from the area of treatment and become tumorigenic [17, 18]. Combining the desired properties of the biomaterials and cells, synthetic scaffolds can be combined with the latter [19]. The stem cells can be predifferentiated, acquiring some of the properties of fully functional cells present in the urethra, such as smooth muscle or the basal part of the urothelium. For this purpose, bioprinting technology allows the utilization [20], supplementing cell-enriched hydrogels with cell sheets or simply seeding cell cultures on the hydrogel surface; these biomaterials can be further reinforced by adding polymeric meshes or nanofibers which could serve a dual structural-drug delivery purpose [21, 22]. Thus, by bioprinting predifferentiated stem cells in mesh-reinforced hydrogels, artificial urethral tissue with a biologically-relevant architecture and mechanical properties can be created.

This study aimed to develop and evaluate a multilayered, cell-laden hydrogel scaffold designed to closely mimic the native structure of the urethra. By combining predifferentiated buccal mucosa cells and adipose-derived mesenchymal stem cells within a GelMA–silk fibroin (SF) hydrogel reinforced by electrowritten polycaprolactone (PCL) and electrospun polylactic acid (PLA)-PCL meshes, the construct enabled targeted regeneration of both epithelial and smooth muscle layers. In a rabbit model, it demonstrated robust biocompatibility, limited inflammatory responses, and preserved urethral patency with

minimal fibrosis. These results highlight the potential of this complex, spatially organized scaffold as a promising platform for future urethral reconstruction studies, particularly in models of pre-established strictures.

2. Results

2.1. A cell-laden, multilayered scaffold was fabricated to replicate the epithelial and muscular layers of the urethra

To identify a suitable bioink composition for scaffold fabrication, multiple GelMA and SF formulations were evaluated with a primary focus on their practical applicability during implantation. Initially, GelMA-based formulations of varying concentrations were tested; however, it quickly became evident that additional structural reinforcement was required to obtain constructs with sufficient mechanical integrity for surgical handling. For this purpose, SF was introduced to improve internal cohesion of the hydrogel network, which reduced printability but improved mechanical robustness during handling and suturing. Multiple compositions of GelMA (5%, 10%, 15%) with and without the addition of 5% SF were tested, and the compositions were selected empirically based on their printability and suturability. Printability was evaluated by qualitatively assessing filament formation, strand continuity, and structural fidelity after crosslinking, while suturability was evaluated by three urological surgeons assessing the ability of the constructs to withstand surgical manipulation. The results of this qualitative evaluation are summarized in table 1. This approach allowed us to identify 10% GelMA–5% SF as the most suitable formulation, providing a balance between printability and mechanical stability required for implantation.

The empirically selected GelMA–SF composite hydrogel (10% GelMA, 5% SF, 0.1% (w/w) LAP) was used to fabricate artificial urethral tissue (figure 1) as a layered construct composed of a 3D-printed hydrogel scaffold populated with two lineage-directed cell types: epithelial-like cells derived from rabbit buccal mucosa cells (RBMCs, figure 2(a)) and smooth muscle-like cells derived from rabbit adipose stem cells (RASCs, figure 2(b)). RASCs were suspended in the GelMA-SF hydrogel at a density of 5×10^6 cells/ml and bioprinted to form the 200–300 μm thick wall of the structure, followed by 5 d of culture in smooth muscle differentiation medium. In parallel, RBMCs were expanded and differentiated separately, and subsequently seeded onto the luminal surface at a density of 5×10^5 cells cm^{-2} to form the epithelial layer, completing the multilayered architecture.

The acellular GelMA–SF hydrogel exhibited a local Young's modulus of 16.6 $\pm$ 4.7 kPa, as assessed by atomic force microscopy (AFM). In the cell-laden GelMA-SF hydrogel, local stiffness decreased to 9.3 $\pm$ 2.6 kPa. In comparison with AFM-derived stiffness measurements reported for native and fibrotic urethral tissue, the cell-laden GelMA-SF hydrogel showed a local stiffness closer to normal urethral matrix than to fibrotic urethral stricture tissue and remained markedly below the stiffness reported for stricture scar tissue [23].

Although these local stiffness values support the physiological relevance of the GelMA–SF hydrogel matrix, the constructs were not sufficiently robust to withstand surgical manipulation and suturing without additional reinforcement. To address this limitation, the constructs were reinforced with two types of mesh structures selected according to their fiber architecture, spatial position within the construct, and practical mechanical behavior during handling and suturing. A crosshatched PCL mesh, produced via melt electrowriting (MESW) and composed of relatively thick fibers of approximately 15 μm (figure 2(c)), was affixed to the luminal surface (figure 2(d)). In contrast, a nanofibrous PLA–PCL mesh, fabricated via solution electrospinning (SES) and composed of finer fibers of approximately 1 μm, was applied to the outer, wall-facing side of the construct (figure 2(e)). This reinforcement strategy was designed to provide temporary mechanical support during implantation and early healing without compromising the biological functionality of the hydrogel. The luminal PCL mesh primarily served a protective role, maintaining structural integrity of the epithelial-facing layer, while the outer PLA–PCL mesh provided additional mechanical support to facilitate suturing and handling. This design decision was supported by qualitative assessment of construct handling and suturability (table 1), where unreinforced hydrogels were consistently insufficient for surgical use, whereas reinforced constructs demonstrated improved structural integrity during manipulation. A representative image of the final multilayered, surgically implantable construct is shown in figure 2(f).

To evaluate cell phenotype following directed differentiation, gene expression analysis (quantitative PCR (qPCR)) was performed on samples collected after 5 d of differentiation but prior to construct assembly. In RBMCs, Ck14 expression decreased 8.8-fold (0.11 $\pm$ 0.02 vs 1.00 $\pm$ 0.20; $p = 0.0004$), while Rptn increased 1.77-fold (1.77 $\pm$ 0.43 vs 1.00 $\pm$ 0.44; $p = 0.0011$) (figure 2(g)). No significant differences were detected for Flg ($p = 0.16$) or Ocln ($p = 0.17$). In RASCs, Acta2 expression increased 2.94-fold in differentiated RASCs (2.94 $\pm$ 1.67) compared to undifferentiated controls (1.00 $\pm$ 0.83; $p = 0.018$), and Cald1 increased 3.78-fold (3.78 $\pm$ 1.35 vs 1.00 $\pm$ 0.30; $p = 0.0003$) (figure 2(h)). These findings indicate successful myogenic and epithelial lineage commitment of RBMCs at the gene expression level. To further confirm lineage-specific protein

Table 1. Qualitative evaluation of bioink printability and construct suturability across GelMA-SF compositions with and without cells and mesh reinforcement. Three printing runs were performed for each composition to assess printability, defined by filament formation, strand continuity, and structural fidelity after crosslinking. Suturability was evaluated by three urology surgeons based on the ability of the constructs to maintain structural integrity during surgical manipulation. Cell-laden constructs contained rabbit adipose stem cells (RASCs) embedded within the hydrogel and rabbit buccal mucosa cells (RBMCs) seeded onto the luminal surface. Mesh-reinforced constructs included a luminal polycaprolactone (PCL) mesh and an outer polylactic acid (PLA)–PCL mesh. The concentration of LAP was kept constant at 0.1% (w/w) in all cases. The grading scale is as follows: '+++'—completely satisfactory, '++'—satisfactory with varying quality, '+'—satisfactory in 2/3 cases, '–'—satisfactory in 1/3 cases, '–'—unsatisfactory with varying quality, '—'—completely unsatisfactory, N/A—the test was not performed as no samples were produced.

GelMA (%)	SF (%)	Cells	Printability	Meshes	Suturability
5%	—	Acellular	+	None	—
10%	—	Acellular	+++	None	—
15%	—	Acellular	—	None	+
5%	5%	Acellular	—	None	—
10%	5%	Acellular	++	None	++
15%	5%	Acellular	—	None	N/A
10%	5%	Cell-laden	++	None	+
10%	5%	Acellular	++	Dual-mesh	++
10%	5%	Cell-laden	++	Dual mesh	++

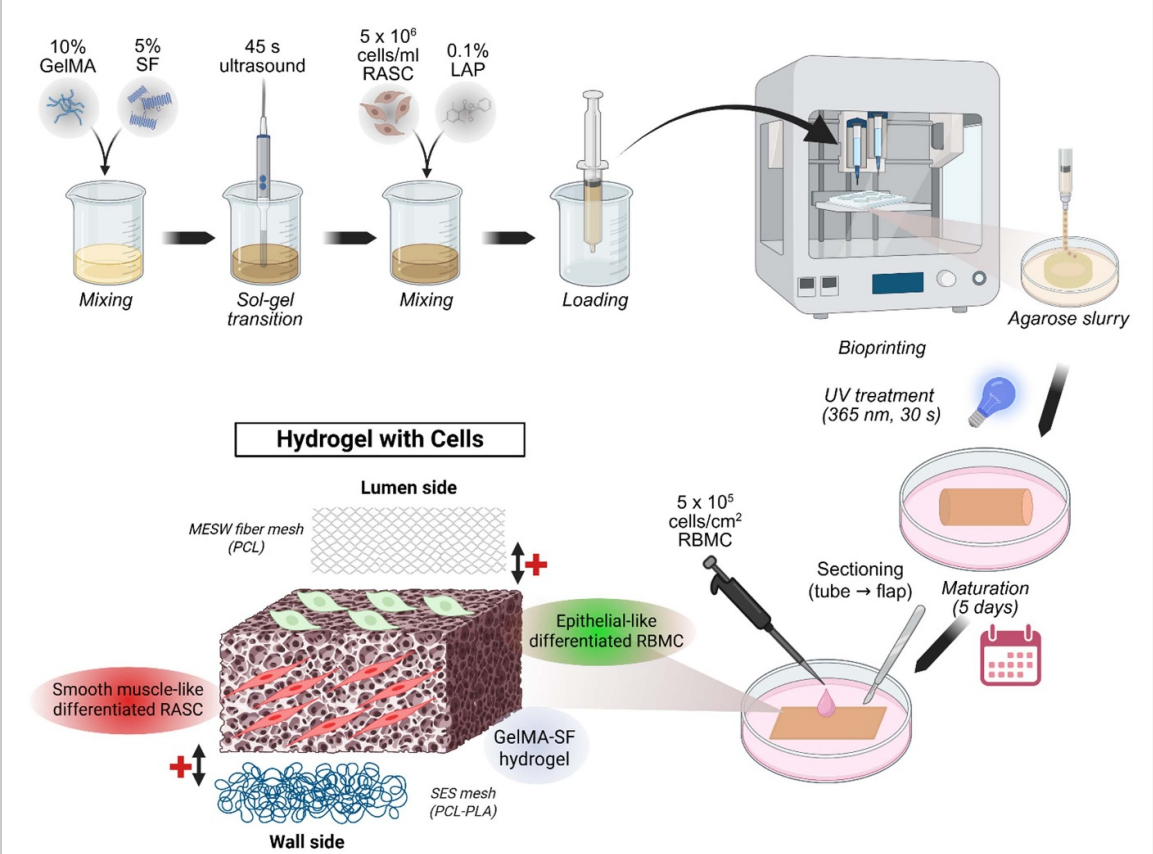


Figure 1. Schematic representation of the manufacturing process of the hydrogel with cells.

expression, immunocytochemistry was performed on assembled constructs without mechanical mesh reinforcement. Cells within the hydrogel stained positive for α-smooth muscle actin (αSMA), indicating RASC differentiation (figure 2(c)), while RBMCs seeded on the luminal surface expressed cytokeratin 14 (CK14), consistent with epithelial identity (figure 2(b)).

2.2. Leukocyte hematological profile revealed time—and scaffold-dependent immune activation following urethral implantation

After successfully validating the assembled scaffold composition—including cell lineage specification and mechanical performance—we proceeded with *in vivo* evaluation using a rabbit model (figure 3(a), study timeline). The constructs were implanted into

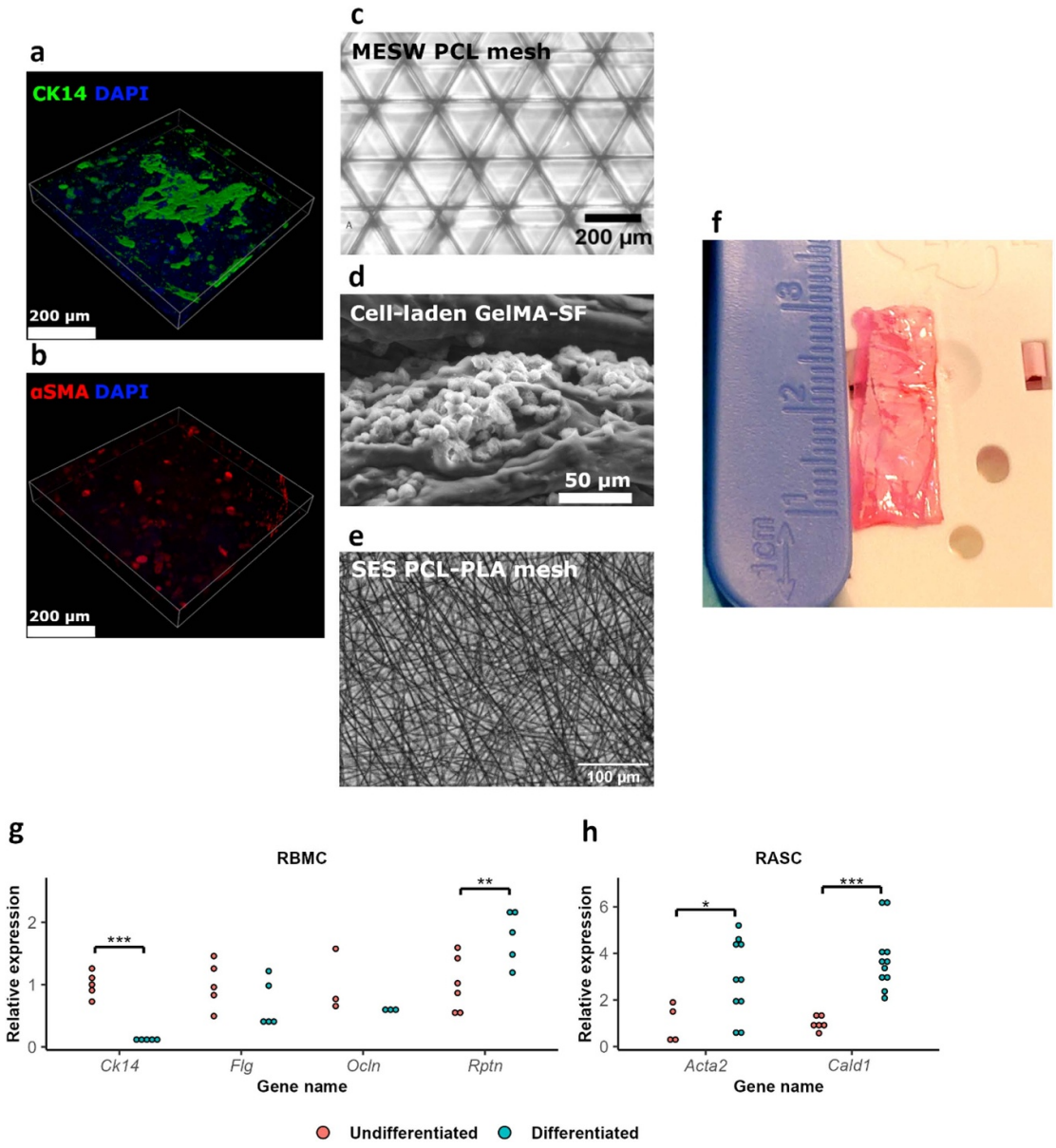


Figure 2. Components and structure of the artificial urethral tissue. a—schematic diagram of the cell-laden artificial urethral tissue. b, c—immunocytochemistry images of, respectively, the top layer (lumen-facing) of the cell-laden scaffold, showing CK14-positive predifferentiated RBMC, and the bottom layer (wall-facing), showing αSMA-positive predifferentiated RASC. d—light microscopy image of PCL mesh manufactured by MESW. e—scanning electron microscopy image of cell-laden artificial urethral tissue. f—light microscopy of PCL-PLA mesh manufactured by SES. g—relative gene expression levels of Ck14, Flg, Ocln and Rptn genes in 5 d differentiated and undifferentiated RBMC. h—relative gene expression levels of Acta2 and Cald in 5-day differentiated and undifferentiated RASC. Gene expression levels standardized to the expression of Gapdh. Dots represent data points. ** marks $p < 0.01$, *** marks $p < 0.001$ calculated using one-way ANOVA. $N = 3$–11, depending on the experimental group. i—picture of the complete artificial graft (hydrogel with cells) prior to implantation.

the mid-penile urethra of male rabbits, mimicking clinical stricture repair techniques (figures 3(b)–(f)). Animals were randomly assigned to one of three groups: a cell-laden scaffold group (hydrogel with cells), an acellular scaffold group (hydrogel), and a sham-operated control group with no implant (incision control). The average operative time was 70 min in scaffold-implanted animals and 27 min in controls. All procedures were completed successfully, with no intraoperative complications.

To assess systemic responses to the implanted materials, hematological parameters were analyzed at 2, 4, and 12 weeks postoperatively. At 2 weeks, animals implanted with hydrogels with cells exhibited elevated white blood cell (WBC) counts ($11.15 \times 10^3/\mu$l), representing a 1.6-fold increase over the incision control group ($7.16 \times 10^3/\mu$l; $p = 0.033$) (figures 4(a)–(d)). This was accompanied by a 2.1-fold increase in granulocytes ($5.77 \times 10^3/\mu$l vs $2.76 \times 10^3/\mu$l; $p = 0.023$) and a 1.8-fold increase in monocytes ($1.08 \times 10^3/\mu$l vs $0.60 \times 10^3/\mu$l; $p = 0.044$). Lymphocytes numbers were higher ($4.23 \times 10^3/\mu$l vs $3.80 \times 10^3/\mu$l), though not significantly ($p = 0.62$), suggesting an acute innate

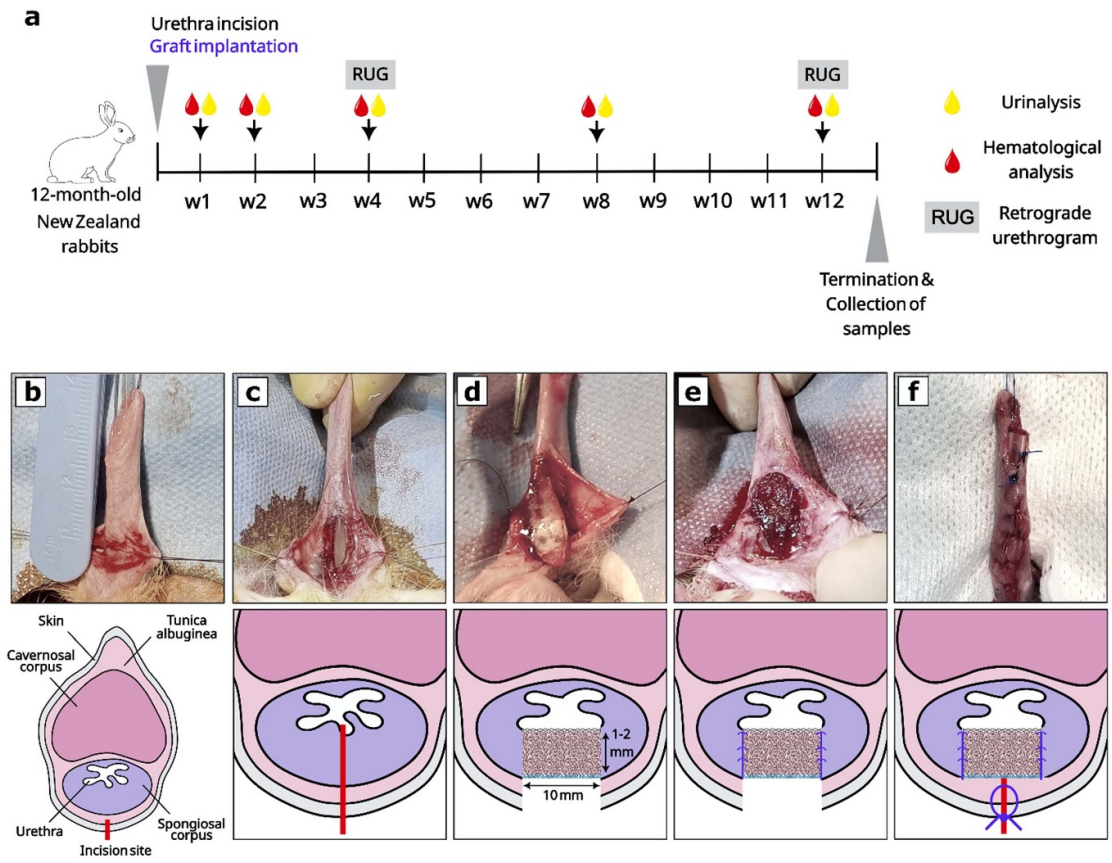


Figure 3. Schematic overview of experiment in vivo phase. a—timeline of postoperative care and scheduled procedures—urine and hematological analyses, retrograde urethrograms (RU) and final histological investigation; bcdef—surgical approach and schematic preview of anatomical structures involved, respectively: b—skin incision, c—urethral incision, d—artificial tissue implantation, e—complete view after tissue implantation, f—final postoperative view with catheter indwelling sutured to the forskin.

immune response to the cell-laden construct. Similar upregulation was also observed in the hydrogel (acellular) group compared to incision control. WBC levels reached 10.10 $\times$ $10^3/\mu$l (1.4-fold; $p = 0.13$), granulocytes 3.38 $\times$ $10^3/\mu$l ($p = 0.64$), and monocytes 0.84 $\times$ $10^3/\mu$l ($p = 0.30$). Notably, lymphocyte counts were significantly elevated (5.88 $\times$ $10^3/\mu$l vs 3.80 $\times$ $10^3/\mu$l; $p = 0.028$), indicating a lymphocyte-skewed response in the absence of cells.

At 4 weeks, both scaffold groups maintained higher WBC levels (hydrogels with cells: 10.62 $\times$ $10^3/\mu$l; hydrogel: 10.08 $\times$ $10^3/\mu$l) relative to control (7.83 $\times$ $10^3/\mu$l), though not significantly ($p > 0.15$). Monocytes and granulocytes remained elevated in both groups but without statistical significance. Lymphocyte counts were again significantly higher in the hydrogel group (5.66 $\times$ $10^3/\mu$l) than in hydrogels with cells (3.78 $\times$ $10^3/\mu$l; $p = 0.038$) and were higher than control (3.73 $\times$ $10^3/\mu$l; $p = 0.053$).

By 12 weeks, the hydrogels with cells group showed a decline in WBC levels (9.25 $\times$ $10^3/\mu$l), while the hydrogel group remained elevated (10.94 $\times$ $10^3/\mu$l), representing a 1.5-fold increase compared to control (7.10 $\times$ $10^3/\mu$l; $p = 0.048$). Lymphocyte counts stayed higher in the hydrogel group (5.48 $\times$ $10^3/\mu$l vs 3.70 $\times$ $10^3/\mu$l), with borderline significance ($p = 0.058$). No significant differences were observed in monocytes or granulocytes across groups at 12 weeks' time point. These findings suggest that the presence of cells within the scaffold induces a pronounced early immune response that attenuates over time, whereas the acellular hydrogel triggers a milder, delayed leukocytic response, potentially related to scaffold degradation. The absence of this delayed response in the cell-laden group may reflect a modulatory effect exerted by the cells or their remnants, potentially dampening later-stage immune activation.

2.3. Red blood cell (RBC) and platelet (PLT) parameters indicate minimal systemic inflammatory or hematological disturbances

In addition to leukocyte profiling, hemoglobin (HGB), hematocrit (HCT), and RBC counts were also evaluated at 2, 4, and 12 weeks postoperatively to monitor for systemic effects of inflammation, blood loss, or impaired erythropoiesis (figures 4(e)–(h)). Across all groups and time points, HGB and HCT values remained within normal physiological ranges with no statistically significant differences detected

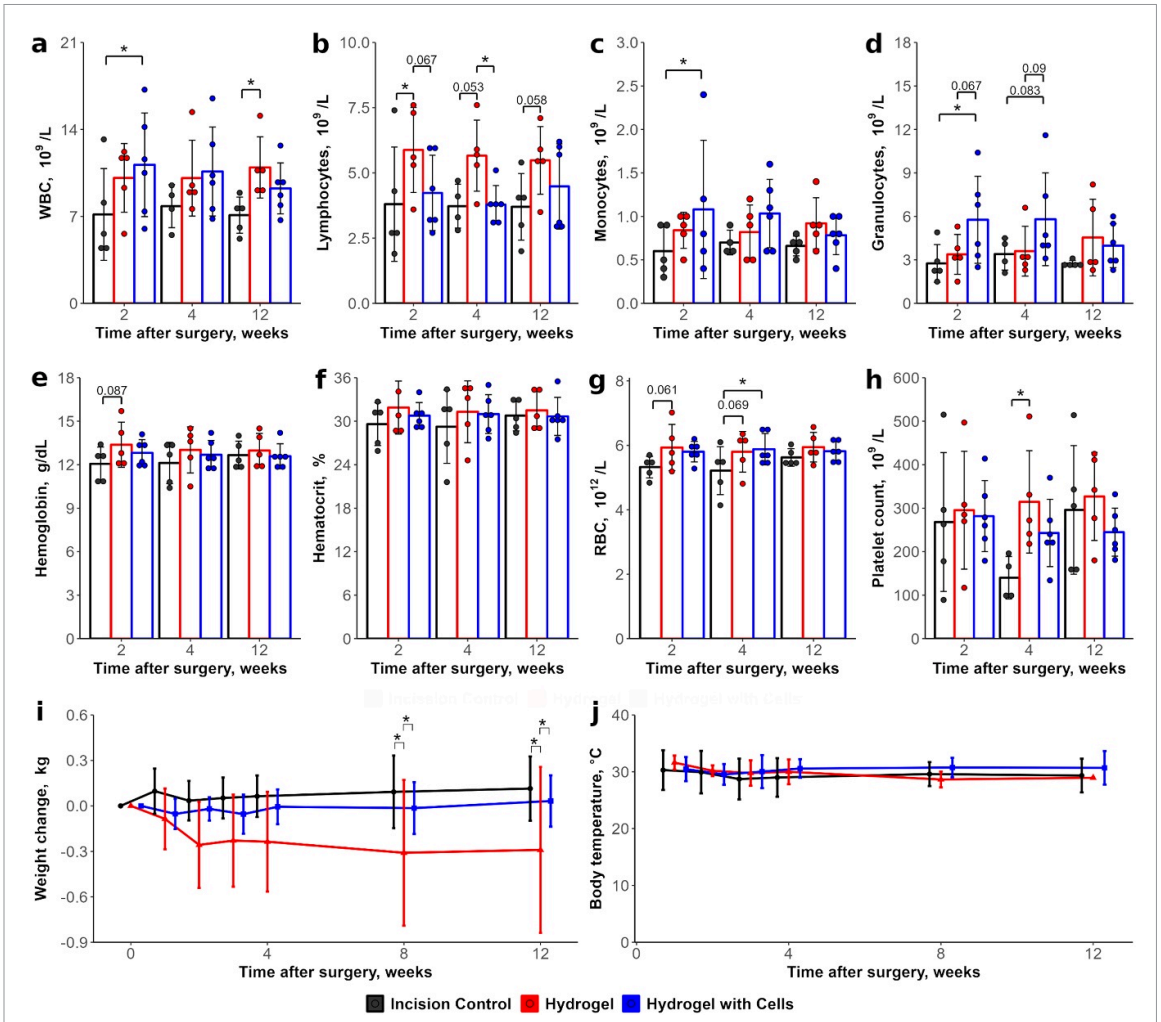


Figure 4. Time-dependent changes in hematological parameters of the artificial urethral tissue implantation. (a)–(d) Dot plots of white blood cells', lymphocytes', Monocytes, and granulocytes counts followed 2, 4 and 12 weeks after surgery respectively. e and f Dot plots of hemoglobin and hematocrit values followed 2, 4 and 12 weeks after surgery respectively. g and h Dot plots of red blood cells and platelet counts followed 2, 4 and 12 weeks after surgery respectively. i line graph indicating the change of animals weight after surgery for 12 weeks. j line graph indicating the body temperature of animals after surgery for 12 weeks. One-way ANOVA, EMM pairwise comparisons. Incision control group N = 5, hydrogel—N = 5, and hydrogel with cells—N = 6, bar height shows group mean, error bars show mean ± SD, dots represent individual animal values. * marks $p < 0.05$.

(all $p > 0.08$ for HGB; $p > 0.26$ for HCT) (figures 4(e) and (f)). RBC counts were similarly stable, except for a modest but statistically significant 1.1-fold increase in the hydrogel with cells group compared to the incision control at 4 weeks ($p = 0.033$) (figure 4(g)). This transient variation did not persist at 12 weeks, suggesting no sustained erythropoietic alteration or inflammation-related anemia.

PLT counts also remained within expected ranges, with high inter-animal variability. A statistically significant increase was observed in the hydrogel group compared to incision control at 4 weeks ($p = 0.021$), but no differences were noted at 2 or 12 weeks ($p > 0.43$) (figure 4(h)). As thrombocytosis can reflect acute phase or inflammatory responses, this transient elevation may suggest mild scaffold-associated reactivity without long-term systemic effects. Overall, the RBC and PLT data do not indicate sustained inflammation, anemia, or clotting abnormalities across experimental groups.

2.4. Body weight loss in the hydrogel group suggests sustained postoperative stress, without accompanying fever or systemic nutritional decline

In addition to hematological parameters, general well-being of animals was assessed by monitoring body weight and body temperature at 1, 2, 3, 4, 8, and 12 weeks postoperatively (figures 4(i) and (j)). Rabbits in the hydrogel group exhibited a gradual decrease in body weight, which became statistically significant by week 8 compared to both the incision control ($p = 0.011$) and hydrogel with cells groups ($p = 0.049$). This trend continued through week 12 ($p = 0.010$ and $p = 0.032$, respectively). One rabbit in the hydrogel group experienced a body weight loss of 15.4% (0.92 kg) within the first postoperative weeks. Additional measures, like improved nutrition and supplementary oral nutrition with syringe stabilized this weight loss and rabbit regained weight with time. Meanwhile, animals in the hydrogel with cells and Control groups either maintained or slightly

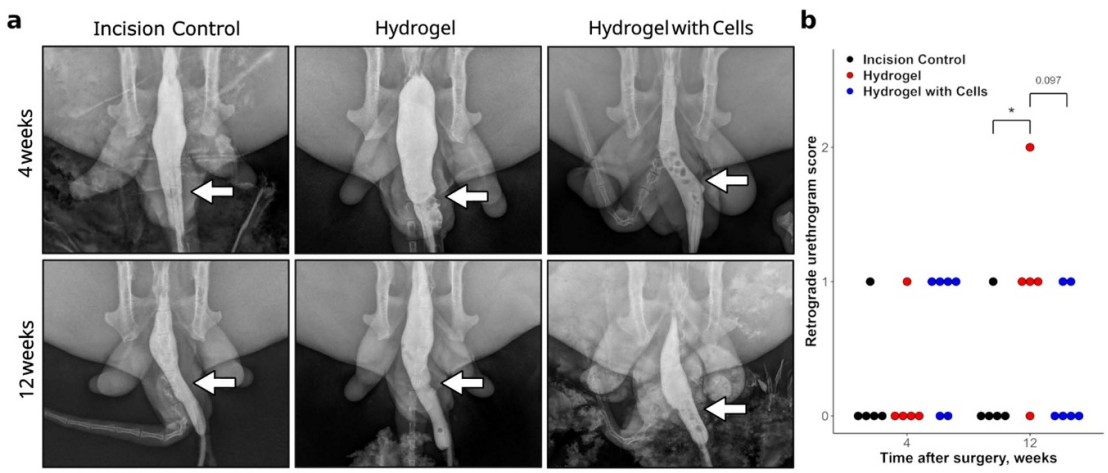


Figure 5. Time-dependent changes in urethrograms post the artificial urethral tissue implantation. (a)—Retrograde urethrograms of control group, hydrogel group and hydrogel with cells group rabbits, 4 weeks and 12 weeks postoperatively. (b)—Dot plots of retrograde urethrogram score followed 4 and 12 weeks after surgery respectively. One-way ANOVA, EMM pairwise comparisons. Incision control group N = 5, hydrogel—N = 5, and hydrogel with cells—N = 6. Dots represent individual animal values. * marks $p < 0.05$.

increased their weight. Body temperature, measured non-invasively at the base of the ear using contactless infrared thermometry, remained stable across all groups and time points (range: 28.6–31.6 °C), with no significant differences detected (all $p > 0.19$), indicating no systemic febrile response or overt infection.

Importantly, values of HGB, HCT, and red blood cell counts remained within physiological ranges and did not differ significantly between groups at any time point. This suggests that, despite observed weight loss in some animals, overall nutritional status, erythropoiesis, and systemic oxygen-carrying capacity were preserved, supporting the conclusion that the animals remained in stable health throughout the study period.

2.5. Clinical signs after scaffold implantation did not show differences between groups

Animals were monitored for core body temperature, behavior, activity, fur condition, urination, defecation, food and water intake, and wound appearance (figure S2). Transient findings included traces of blood in the litter of one incision control rabbit during the first postoperative week and one hydrogel with cells rabbit during the second week, without recurrence thereafter. Reduced feed intake was noted in three hydrogel group rabbits at week 1 but normalized subsequently. Mild fur changes were observed in a few animals from both scaffold groups, while one hydrogel with cells rabbit displayed lower activity during the first 8 weeks. None of these signs were persistent or severe, and no animals showed clinical features indicative of poor overall condition. In addition, urinary biochemical parameters assessed at 2, 4, and 12 weeks postoperatively showed no consistent differences or group-specific trends (figure S3).

2.6. Cell-laden scaffolds support urethral tissue stability and reduce luminal narrowing over time

To assess tissue response and urethral integration following implantation, retrograde urethrograms were performed at 4 and 12 weeks postoperatively (figure 5). Contrast imaging enables visualization of the urethral lumen and detection of structural abnormalities, including narrowing or irregular contours suggesting stricture development (figure 5(a)).

In the hydrogel with cells group, 4 out of 6 animals exhibited mild luminal narrowing at 4 weeks (score 1), but in two of these cases, the urethral profile returned to normal by 12 weeks. No strictures (score 2) were observed at either time point. This suggests progressive integration of the scaffold and minimal adverse remodeling.

In contrast, animals in the hydrogel group demonstrated a worsening profile over time. At 4 weeks, only 1 of 5 animals showed suspected narrowing. However, by 12 weeks, 4 out of 5 animals had elevated scores, including one confirmed case of stricture formation (score 2). This indicates that the acellular hydrogel may have induced localized tissue stress or insufficient integration, leading to progressive narrowing.

The incision control group consistently showed normal or near-normal urethral morphology at both time points, with no strictures recorded. Statistical comparison revealed a significant difference between the hydrogel and Control groups at 12 weeks ($p < 0.05$), and a trend toward lower scores in the hydrogel with cells group compared to the hydrogel-only group ($p = 0.097$) (figure 5(b)).

Taken together, these findings suggest that cell-laden scaffolds may facilitate more favorable urethral healing, limiting fibrotic narrowing and promoting stable lumen architecture over time.

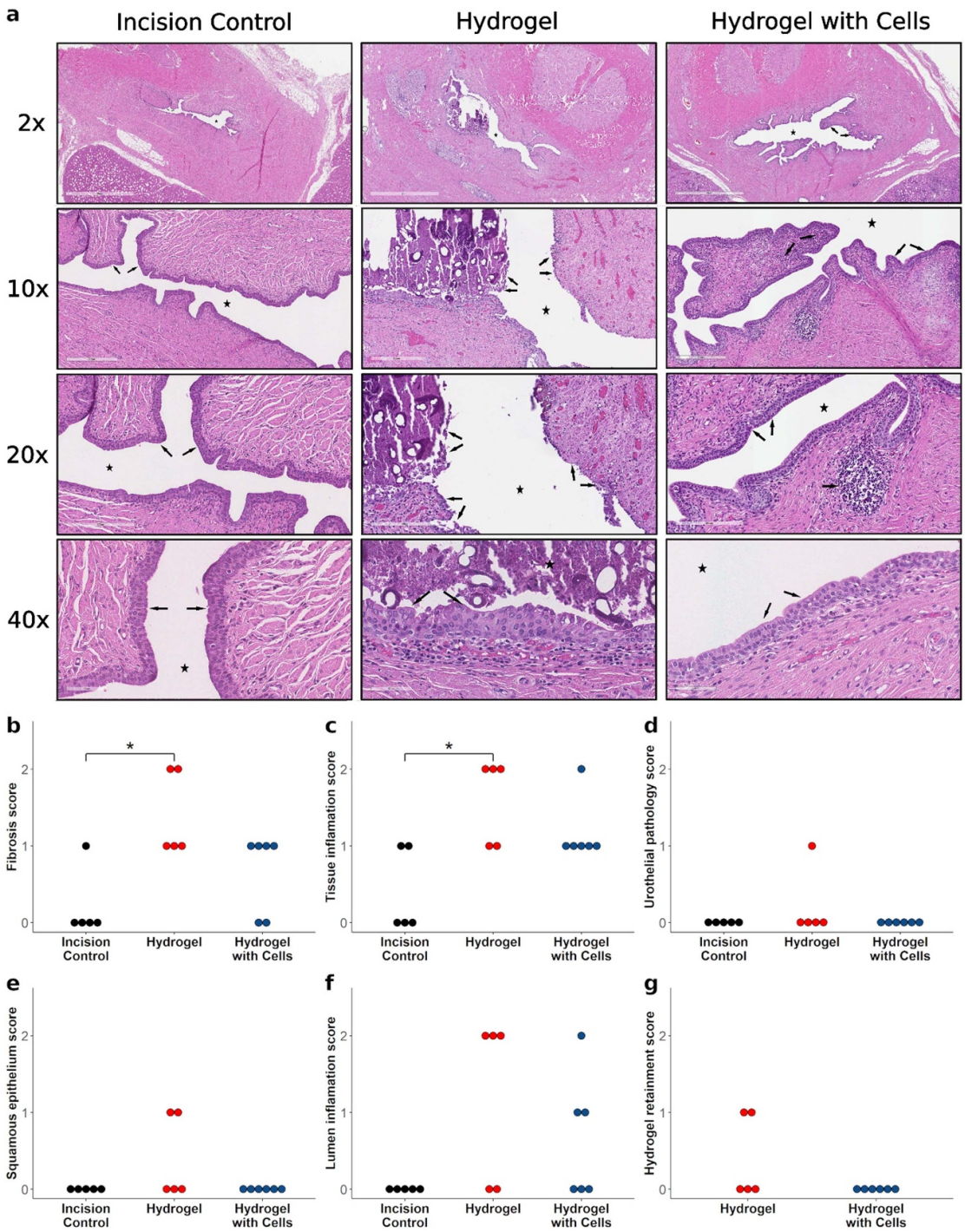


Figure 6. Histology. a—specimens of incision control, hydrogel and hydrogel with cells groups after hematoxylin and eosin (H&E) staining at 2x,4x,10x and 20x imagination. Findings were evaluated in 0–2 scale, 2 mean clearly expressed finding, 1—suspicious, 0—finding was not observed. Dot plots of pathological evaluation score: b—fibrosis score; c—tissue inflammation score; d—urothelial pathology score; e- squamous epithelium score; lumen inflammation score; g—hydrogel retainment score. One-way ANOVA, EMM pairwise comparisons. Incision control group $N = 5$, hydrogel—$N = 5$, and hydrogel with cells—$N = 6$. Dots represent individual animal values. * marks $p < 0.05$.

2.7. Cell-laden scaffolds are associated with a lower adverse tissue response than acellular hydrogels

To further investigate scaffold–tissue interactions and assess tissue remodeling, histological analyses of excised urethras were performed at 12 weeks post-operatively (figure 6(a)). In the hydrogel with cells group, inflammatory changes were observed in only 1 of 6 rabbits, and fibrosis was seen in 2 of 6. No residual hydrogel material was detected in any case. Urethral patency, defined by an unobstructed lumen and intact urothelial lining, was confirmed in 4 of 6 animals. All samples retained normal transitional epithelium architecture, and no evidence of stratified squamous epithelium was detected, indicating limited chronic irritation or epithelial remodeling.

In contrast, histological sections from the hydrogel group revealed inflammatory infiltration in 3 of 5 rabbits and fibrosis in 4 of 5, both significantly more frequent than in the incision control group (figures 6(b) and (c); $p = 0.016$ for both). Atypical epithelial changes were observed in 3 of 5 animals, including reactive urothelial atypia (figure 6(d)) and focal areas of stratified squamous epithelium replacement, though differences between groups did not reach statistical significance (figure 6(e); $p = 0.192$ vs incision control). Intraluminal neutrophilic infiltration was also evident in 2 of 5 cases (figure 6(f)). Urethral patency was preserved in only 1 of 5 samples. Residual hydrogel material was identified in 1 of 5 samples, surrounded by foreign-body giant cells and macrophages (figure 6(g)). In the incision control group, histological assessment revealed well-organized urothelium with minimal mononuclear cell infiltration and no fibrosis or epithelial remodeling. No stratified squamous epithelium or residual surgical artifacts were identified. Together, these results suggest that incorporation of cells into the hydrogel was associated with a lower frequency of adverse tissue responses than the acellular scaffold, including inflammation, fibrosis, and epithelial alterations, although fibrosis was not completely prevented in the hydrogel with cells group.

3. Discussion

Although urethral strictures are relatively common and have been studied for centuries, their pathology and treatment are still under research. Endoscopic internal urethrotomy, urethral stents, dilations, and antifibrotic drug injections are successful in the short term but ineffective in the long term [24]. The most popular treatment, direct vision internal urethrotomy (DVIU), has a failure rate of 61.4% at 24 months after surgery [25]. The outcomes of repeat DVIUs and strictures greater than 2 cm are even worse. Open urethroplasty remains the gold standard for the treatment of strictures. For advanced strictures that cannot be removed and an initial anastomosis formed, free graft urethroplasty (FGU) is the procedure of choice, and the BMG is currently the most widely used graft [26]. The patency rate for bulbar urethral FGU is 88%–91%, with a follow-up period of 12–40 months [27]. There is some evidence that patency rates decline over time. Subset analysis of the 4 select and homogeneous studies noted 1, 5, 10, and 15 years stricture free survival rates of 0.97, 0.96, 0.74, and 0.63, respectively [28]. The main disadvantage of BMG harvesting is the oral morbidity. BMG harvesting provokes oral tightness which can be presented in up to 24% of patients after six months [29]. Numbness (61%), difficulty in chewing (54%), swelling (48%) and articulation (40%) were the most common problems during the first week [30]. Penile skin is another popular type of graft, especially in uncircumcised men, where the foreskin is a rich source of graft material. Although the results of BMG augmented urethroplasty and penile skin graft urethroplasty are similar [31], penile skin grafting has its drawbacks. Confounding factors include cosmetic defect, limited amount of bare skin, and donor site morbidity [32]. Skin diseases such as lichen sclerosus are contraindications to penile skin grafting urethroplasty [33].

As an alternative, tissue-engineered grafts appear to be a promising source of available material. The main advantages of bioengineered tissues are relatively unlimited tissue supply, reduced donor site morbidity, and biocompatibility. Our aim was to use artificial scaffolds enriched with predifferentiated cells to ensure a successful healing process and the positive well-being of the model organism. In practice, both undifferentiated and differentiated stem cells have shown therapeutic benefits [34]. The use of undifferentiated stem cells for treating urethral strictures has antifibrotic effects—likely due to their immunomodulatory properties [35, 36]—however, this type of treatment has potential side effects of tumorigenicity, as the implanted stem cells can migrate and form malignancies in various parts of the host, or simply die in the unsupportive environment without long-term therapeutic benefit [17, 18, 37]. The strategy to avoid this was to predifferentiate the cells towards the functional cell types of the urethra. We aimed to achieve guided regeneration, as the implanted predifferentiated cells would not migrate from the urethra, substitute for the urethral tissues and elicit a healing effect—a concept developed for bone regeneration [38]. Further differentiation of stem cells, attempting to produce the stratified subtypes of the urothelium in the laboratory is also possible, however, this would significantly extend and complicate the manufacturing procedure, reducing the effectiveness and applicability of the treatment we investigated.

To regenerate the urothelium, we chose a well-established cell source isolated from buccal mucosa tissue. Buccal mucosa remains the gold standard in urethroplasty for repairing large urethral defects, as this tissue integrates effectively and restores the urothelial barrier function [39, 40]. To reconstruct the smooth muscle layer of the urethra, essential for elasticity and mechanical stability, we used adipose-derived mesenchymal stem cells. This cell source has been extensively studied in urethral tissue engineering due to its ready availability, ease of isolation and maintenance, and broad differentiation potential [16, 41, 42]. Moreover, these cells are known for their immunomodulatory and antifibrotic properties, which are particularly valuable in urethral regeneration [36, 43]. To guide regeneration more

precisely, prior to implantation, we pre-differentiated both cell types toward their target phenotypes, with RBMCs and RASCs expressing urothelium-specific markers (cytokeratin 14 (CK14), Rptn) and smooth muscle markers (smooth muscle actin (αSMA), Acta2, Cald1), respectively, prior to the implantation of the artificial tissue.

While supplementation of GelMA with silk fibroin is a widely used strategy to improve hydrogel cohesion and mechanical performance [44], the resulting GelMA–SF hydrogel showed different local stiffness depending on whether cells were incorporated. AFM analysis showed that the acellular GelMA–SF hydrogel had a local stiffness of 16.6 $\pm$ 4.7 kPa, whereas incorporation of adipose-derived cells reduced the local stiffness to 9.3 $\pm$ 2.6 kPa. For comparison, Li *et al* reported AFM-derived stiffness values of 5.23 $\pm$ 0.37 kPa for normal human urethra and 41.59 $\pm$ 2.48 kPa for human urethral stricture scar tissue [23]. In this context, the cell-laden hydrogel was closer to the low-kPa stiffness of native urethral tissue, while the acellular hydrogel was positioned between native and fibrotic urethral matrix stiffness values. However, these measurements reflect local hydrogel matrix stiffness rather than the bulk mechanical behavior of the complete construct. Despite this favorable local matrix stiffness, the GelMA-SF hydrogel remained too soft and fragile for direct surgical manipulation. Therefore, the constructs were reinforced with two types of meshes fabricated from FDA-approved polymers [45–47]: an electrospun PCL–PLA co-polymer mesh on the host tissue-facing side and a melt electrowritten PCL mesh on the luminal side. This multilayered design combined a cell-supportive hydrogel matrix with structural reinforcement, enabling secure suturing into the urethral defect without compromising construct integrity.

Scaffold implantation surgeries required different durations across the groups. Procedures in the incision-only control group took approximately 27 min on average, whereas operations involving scaffold implantation—either with or without cells—lasted nearly twice as long, averaging about 70 min. However, based on our overall postoperative assessments, these longer operation times did not appear to have any significant systemic impact on the animals. HCT, HGB, and RBC levels remained stable throughout the study, indicating no chronic blood loss or signs of nutritional compromise [48]. In contrast, we observed distinct immune profiles between animal groups. Rabbits implanted with cell-laden scaffolds demonstrated an early, transient elevation in leukocytes, monocytes, and granulocytes, which normalized by 12 weeks. This pattern is consistent with previous studies on cell-seeded scaffolds, where an initial immune response is typically attributed to recognition of transplanted cells or the clearance of apoptotic material [49, 50]. Meanwhile, animals receiving acellular hydrogel implants exhibited a delayed increase in leukocyte counts, suggesting a mild chronic inflammatory response, possibly due to ongoing scaffold degradation—an outcome also reported in other works [49, 51, 52]. Unlike studies that noted sustained leukocytosis beyond 12 weeks [53], we found that immune markers had returned to baseline by the study endpoint. Changes in body weight further supported these observations. Rabbits implanted with acellular hydrogels experienced greater weight loss over time, reaching statistical significance at later intervals, which may reflect increased metabolic demands associated with prolonged inflammation [54]. In contrast, animals receiving cell-laden scaffolds maintained more stable body weights, likely related to the known immunomodulatory and antifibrotic properties of adipose-derived mesenchymal stem cells [55, 56]. Throughout the study, no febrile responses were recorded, indicating the absence of systemic infection. Urinalysis and behavioral monitoring similarly revealed no concerning differences between groups, with all parameters remaining within physiological ranges. Taken together, these findings suggest that while inclusion of cells temporarily amplified the early immune response, it may have contributed to reducing long-term inflammatory effects often seen with acellular constructs.

Histological analysis together with urethrogram imaging indicated that the artificial tissue containing pre-differentiated cells was well tolerated by the host, showing minimal long-term inflammation, reduced fibrosis, and preservation of urethral lumen architecture compared to acellular constructs. Retrograde urethrograms performed at 4 and 12 weeks confirmed that most rabbits receiving cell-laden scaffolds maintained an open urethral lumen without notable narrowing. In contrast, animals implanted with acellular hydrogels exhibited more frequent inflammatory infiltrates and fibrotic changes on histology, along with a higher incidence of urethral narrowing on imaging. These findings are consistent with reports that unseeded biomaterial scaffolds can lead to prolonged immune responses and fibrotic remodeling [49, 51, 57, 58]. No fistulas or severe complications were observed in any group, suggesting that all implantation approaches were generally safe. Overall, these results indicate that integrating pre-differentiated epithelial and smooth muscle-like cells within the scaffold may guide more organized tissue regeneration and reduce adverse remodeling.

Most studies in urethral tissue engineering have focused on single-component scaffolds, typically relying on decellularized matrices [59–61], hydrogels [62–65], or, in some cases, purely synthetic polymers [65, 66]. However, each of these material choices comes with inherent drawbacks. This is particularly

relevant given that the urethra is a sophisticated tissue composed of multiple functionally specialized layers, which simpler scaffolds cannot fully replicate [68–70]. For this reason, we opted for a more complex scaffold architecture, combining a GelMA hydrogel reinforced with SF and two types of electrospun meshes for structural support. While each of these materials has been individually explored in regenerative medicine [59, 71–74], they have not been integrated together into a single urethral construct. This composite design enabled us to harness the advantages of each component—providing a supportive matrix for cell migration and proliferation, enhancing mechanical strength, and improving surgical handling—while minimizing their individual limitations.

Beyond the scaffold's composite architecture, a key distinguishing element of our study was the combined spatial and phenotypic control achieved through the use of two complementary cell types: buccal mucosa–derived cells for urothelial regeneration and adipose-derived mesenchymal stem cells for smooth muscle reconstruction. While most urethral tissue engineering studies continue to focus on acellular constructs or employ a single cell type distributed uniformly throughout the scaffold [75–78], a smaller subset has explored combining multiple cell sources, such as urothelial cells with smooth muscle cells or muscle cells with lingual keratinocytes [79]. However, these strategies generally involve fully differentiated cells isolated directly from donor tissues, without additional preconditioning toward their regenerative lineage. In contrast, our approach integrated pre-differentiated cell populations, each positioned within a distinct scaffold compartment to mimic native urethral histoarchitecture, aiming to more precisely guide regeneration and improve functional integration [80, 81]. This multilayered, phenotype-targeted construct thus represents an advancement over conventional designs by simultaneously addressing structural, cellular, and spatial aspects of urethral tissue reconstruction [68].

Despite the promising outcomes demonstrated in this study, several limitations and opportunities for future work remain. While we previously confirmed that implanted cells from similar constructs could survive up to 12 weeks and even migrate within host tissue [82], in this study we did not specifically repeat such tracking here; extending these investigations with more detailed spatial and temporal cell fate analyses could strengthen understanding of long-term cellular dynamics. In addition, the present study did not include post-implantation molecular analysis of urothelial maturation, epithelial barrier integrity, or smooth muscle-like tissue organization. Therefore, although H&E histology, urethrograms, and sustained urination throughout the 12-week follow-up support epithelial continuity and urethral patency in the hydrogel with cells group, the molecular mechanisms underlying tissue organization and barrier restoration remain to be defined in future studies. The mechanical and printing-related characterization of the construct was also limited to application-driven functional assessment rather than comprehensive quantitative material testing. Printability and suturability were evaluated qualitatively during scaffold fabrication and surgical handling, and AFM was used to assess local hydrogel matrix stiffness; however, rheological, photorheological, DMA-based, tensile, and suture-retention measurements of the bioink, isolated meshes, and complete mesh-reinforced construct were not performed. These analyses will be required in future dedicated optimization studies to better define ink flow behavior, crosslinking kinetics, bulk mechanical performance, and surgical handling limits. Moreover, although our current study was designed to assess biocompatibility and integration in healthy urethral tissue, it should be interpreted as a proof-of-concept demonstrating the feasibility and biological performance of the proposed construct *in vivo*. Future experiments applying this construct to pre-formed urethral strictures would better emulate the clinical scenario, providing insight into the scaffold's true regenerative and anti-fibrotic capacity. Finally, although we demonstrated stable urethral architecture and a lower frequency of fibrosis in the hydrogel with cells group compared with acellular hydrogels, functional assessments, such as urodynamic measurements, are essential to confirm the restoration of physiological urine flow and pressure. Looking ahead, the use of our synthetic meshes not only for structural support but also as platforms for localized delivery of antifibrotic or anti-inflammatory agents presents a particularly intriguing strategy to further enhance therapeutic outcomes.

Taken together, our approach—integrating a multi-layered composite scaffold with spatially organized, pre-differentiated cell types—stands in contrast to many previous studies that have employed simpler architectures or single-cell populations [75–78]. Unlike earlier efforts in urethral tissue engineering, which have shown limited success with acellular or single-cell-type constructs [83], our strategy aims to address key challenges in tissue engineering, such as poor tissue integration, persistent inflammation, and incomplete regeneration of functional layers, which often lead to complications like fibrosis and luminal narrowing. By contrast, our study showed that employing two distinct, lineage-committed cell populations within tailored hydrogel compartments promoted more physiologically relevant tissue regeneration. Specifically, we observed reduced inflammatory infiltration, less fibrosis, and more frequent preservation of an open urethral lumen compared to constructs lacking cells—direct evidence that

our combined strategy enhanced biocompatibility and scaffold integration. Notably, the architecture itself, with targeted placement of epithelial-like and smooth muscle-like layers, likely played a pivotal role in supporting site-specific regeneration, as suggested by the absence of organized urothelium in acellular scaffolds. This underscores the importance of both phenotype-specific pre-differentiation and multi-compartment scaffold design in achieving more robust, functionally oriented urethral repair—an advancement over prior studies that did not address these complexities [83].

4. Materials and methods

4.1. Cell cultures

Artificial urethral grafts were engineered using cells isolated from adipose and buccal mucosal tissues of adult male New Zealand White rabbits (Oryctolagus cuniculus, Animalab Hungary Kft.). The animals used in the study were approximately 12 months old, with an average weight of 4.5 ± 0.3 kg.

All animal procedures were approved by the State Food and Veterinary Service of Lithuania (permit No. G2-158, issued 2020–09–16) and conducted in accordance with national regulations and EU Directive 2010/63/EU on the protection of animals used for scientific purposes.

Anesthesia was induced via intramuscular injection of ketamine hydrochloride (35 mg kg^{-1}, Bioketan, Vetoquinol) and xylazine (5 mg kg^{-1}, Xylamed™, Bimeda). The perineal region was sterilized using a 10% povidone-iodine solution followed by a 0.1% octenidine dihydrochloride with 2% phenoxyethanol solution. Sterilization of the oral cavity was not required prior to biopsy collection.

To establish RASC cultures, approximately 30 mm^3 of adipose tissue was harvested from the perineal region. The tissue was rinsed in Hanks' Balanced Salt Solution (HBSS; Gibco), mechanically minced, and enzymatically digested with collagenase I (Gibco) at 37 °C for 2 h. Following digestion, the suspension was pipetted thoroughly using a 200 μl pipette and centrifuged at 600 × g for 10 min. The supernatant was discarded, and the cell pellet was resuspended in RASC culture medium composed of Iscove's Modified Dulbecco's Medium (IMDM; Gibco) supplemented with 10% fetal bovine serum (FBS; Gibco) and 1% penicillin-streptomycin (Gibco). Cells were seeded into 12-well plates. For RBMC cultures, a 5 × 5 mm biopsy of buccal mucosa was excised from the inner oral surface. The sample was washed with HBSS, mechanically dissociated, and enzymatically digested in collagenase I (Gibco) at 37 °C for 1 h. The resulting cell suspension was pipetted thoroughly and centrifuged at 400 × g for 5 min. Cells were cultured in RBMC medium consisting of DMEM/F12 (Gibco) supplemented with 5% FBS, 1% insulin-transferrin-selenium (ITS; Gibco), 1% penicillin-streptomycin, 10 ng ml^{-1} β-nerve growth factor (βNGF; Peprotech), 5 ng ml^{-1} epidermal growth factor (EGF; Peprotech), and 200 ng ml^{-1} hydrocortisone (Sigma-Aldrich). Once adherent, proliferating colonies were observed, and cells were passaged using 0.1% trypsin-EDTA (Gibco) and transferred to T25 culture flasks (TPP) for further expansion.

The established cell cultures were maintained in 37 °C, 5% CO_2 atmosphere incubator (Thermo Fisher). Once confluent, the cell cultures were washed twice with PBS, trypsinized using 0.1% trypsin-EDTA, diluted at a ratio of 1:3 in regular culture medium and split into new flasks.

To differentiate RBMC towards epithelium, the regular culture medium was changed to LG-DMEM (Gibco) medium containing 0.5% Ultroser, 1% ITS, 2.5 μg ml^{-1} retinoic acid (Peprotech), 10 ng ml^{-1} keratinocyte growth factor (KGF; Peprotech), 10 ng ml^{-1} hepatocyte growth factor (HGF; Peprotech), 20 ng ml^{-1} EGF and 500 ng ml^{-1} hydrocortisone. To differentiate RASC towards smooth muscle, the culture medium was exchanged for LG-DMEM with 0.5% Ultroser, 1% penicilin-streptomycin, and 10 ng ml^{-1} transforming growth factor-β1 (TGFβ1; Peprotech).

4.2. Manufacturing of acellular and cell-laden artificial urethral tissue

Artificial urethral tissues were fabricated using a RegenHU Discovery Evolution 3D bioprinter. The hydrogel scaffold was composed of methacrylated gelatin (GelMA; CellINK) and silk fibroin (SF; Advanced Biomatrix) at concentrations of 10% and 5% (w/w), respectively. Lithium phenyl-2,4,6-trimethylbenzoylphosphinate (LAP; 0.1% w/w) served as the photoinitiator. The mixture was ultrasound-treated to induce beta-sheet formation for 45 s per ml of ink using sonicator with the amplitude set at 30%. For manufacturing the hydrogel with cells, 100 μl of the RASC suspension (5.5 × 106 cells) was then carefully pipetted into the mixture; otherwise, the same volume of PBS was added. The bioink was printed via plunger syringe in ambient temperature at a pressure of 60–120 kPa into a 1% agarose slurry mold73 to form tubular structures measuring 20 mm in height and 10 mm in diameter. The construct was crosslinked for 30 s using the bioprinter-integrated UV LED module (365 nm) positioned 1 cm above the final printed layer.

4.3. qPCR

qPCR was conducted to confirm epithelial and mesenchymal differentiation of stem cells cultured within the engineered scaffold. Cells were cultured in differentiation media for 5 d prior to RNA isolation. For this analysis, RASC were cultured in the GelMA-SF hydrogel at a bioprinting density of

5×10^6 cells ml^{-1}, while RBMC were cultured on gelatin-coated 6-well plates (TPP) at a seeding density 5×10^4 cells/cm^2. RNA was extracted using TRIzol™ Reagent (Invitrogen) according to the manufacturer's protocol. RNA quality was evaluated by RNA electrophoresis in a 2% agarose gel. cDNA synthesis was performed using Maxima H Minus First Strand cDNA Synthesis Kit with dsDNase (Thermo Fisher Scientific). qPCR reactions were set up using Luminaris Color HiGreen qPCR Master Mix (Thermo Fisher Scientific) and run on a QuantStudio™ 3 Real-Time PCR System (Applied Biosystems). Thermal cycling conditions were as follows: UDG activation: 50 °C for 2 min; initial denaturation: 95 °C for 10 min; amplification: 40 cycles of 95 °C for 15 s, 60 °C for 30 s and 72 °C for 30 s; melt curve analysis. Gene expression was analyzed using the $\Delta\Delta Ct$ method, with GAPDH used as the housekeeping gene for normalization. Relative expression was calculated for genes listed in table S1 to assess lineage-specific differentiation.

4.4. Immunocytochemistry

Immunocytochemical staining was used to assess epithelial and mesenchymal marker expression within engineered urethral constructs composed of bioprinted RASC and RBMC. RASC were encapsulated in hydrogel during bioprinting, as previously described, and subsequently cultured within the hydrogel in differentiation medium. In parallel, RBMC were cultured on standard tissue culture plastic in differentiation medium at a seeding density of 5×10^4 cells ml^{-1} for 5 d to induce epithelial differentiation. Following differentiation, RBMC were enzymatically detached using 0.4% trypsin-EDTA, the trypsin was deactivated with Soybean Trypsin Inhibitor (Gibco), the cells centrifuged at 300 x g for 4 mins and seeded onto the luminal surface of the hydrogel constructs already containing predifferentiated RASC at a density of 1×10^6 cells/cm^2. The fully assembled, cell-laden constructs were then cultured in DMEM supplemented with 1% Ultroser overnight before fixation. Constructs were washed three times with phosphate-buffered saline (PBS; Roth), 5 min per wash, and fixed overnight at 4 °C in 4% paraformaldehyde (PFA; Roth). Fixed samples were again washed in PBS and permeabilized in 0.3% Tween-20 in PBS (PBST; Sigma-Aldrich) for 2 h at room temperature (RT). Blocking was performed using PBST containing 10% goat serum (Sigma-Aldrich) and 0.3 M glycine (Roth) for 6 h at RT. Constructs were then incubated with primary antibodies for 24 h at 4 °C: Anti-α-smooth muscle actin (αSMA; 1:100, MA10610, Thermo Fisher Scientific) for identification of muscle-like cells; Anti-cytokeratin 14 (CK14; 1:200, EPR17350, Abcam) for epithelial-like cell detection. After incubation, constructs were washed three times with PBS and incubated with Alexa Fluor 594-conjugated goat anti-mouse secondary antibody (1:200, A21135, Thermo Fisher Scientific) for 24 h at 4 °C. Nuclear staining was performed using DAPI (1 μg ml^{-1} in PBS; Sigma-Aldrich) for 1 h at RT. Samples were washed with PBS, mounted on glass slides, and coverslipped using polyvinyl alcohol mounting medium (Mowiol; Roth). Fluorescent images were acquired and processed using Leica SP8 confocal microscope.

4.5. Surgical procedure

Sixteen adult male New Zealand White rabbits (Oryctolagus cuniculus) (Animalab, Hungary Kft.) were randomized into three experimental groups (table S2) using the RAND() function in Microsoft Excel: incision control, hydrogel, and hydrogel with cells. The incision control group served as the surgical control, in which a fusiform urethral defect was created and closed by primary suturing without scaffold implantation. In the hydrogel and hydrogel with cells groups, the corresponding acellular or cell-laden scaffold was implanted into the created urethral defect. The number of animals per group was determined using *a priori* power analysis conducted in G*Power (v3.1), assuming a large effect size ($f = 0.4$), power (β) of 0.8, and significance level (α) of 0.05 for a one-way ANOVA. The rabbits had an average age of 12 months and a mean weight of 4.507 kg at the start of the study. The individual rabbit was considered the experimental unit within the study.

Anesthesia was induced via intramuscular injection of ketamine hydrochloride (35 mg kg^{-1}, Bioketan, Vetoquinol) and xylazine (5 mg kg^{-1}, Xylamed™, Bimeda). The perineal surgical site was sterilized with 10% povidone-iodine and 0.1% octenidine dihydrochloride with 2% phenoxyethanol. A longitudinal midline incision was made on the ventral surface of the penis. The pendulous urethra was dissected and incised along the ventral midline. A fusiform urethral defect was created, and an artificial scaffold (20 mm × 10 mm) was implanted at the lesion site. The scaffold was sutured to the native urethral wall using 6/0 polydioxanone (PDS) sutures. Skin closure was completed in two layers with 4/0 Vicryl Rapid sutures. To maintain urinary flow and scaffold positioning, a 10 Ch urinary catheter was inserted and secured to the foreskin with sutures for 5 d postoperatively. Single-dose intramuscular antibiotic prophylaxis (enrofloxacin, 2.5 mg kg^{-1}, Bayer) and non-steroidal analgesia (carprofen, 4.0 mg kg^{-1}, Rycarfa, KRKA) were administered during surgery.

4.6. Physiological monitoring and clinical evaluation

Rabbits were housed individually in standard laboratory conditions (22 ± 1 °C temperature, 55 ± 3% humidity, 12 h light/dark cycle) with ad libitum access to standard chow and tap water. Postoperative

wound care and disinfection were carried out daily for the first week, followed by weekly monitoring thereafter. Although the urinary catheters were planned to be removed on postoperative day 5, in reality the catheters were lost on the first postoperative day. Instead, the catheters were sutured to the foreskin, the rabbits removed the catheters as soon as they woke after the surgery.

General health and recovery were monitored using a standardized welfare assessment protocol. Parameters assessed included: core body temperature, measured using a remote contactless infrared thermometer applied to the inner surface of the ear, body weight, recorded at baseline and at postoperative weeks 1, 2, 3, 4, 8, and 12; furthermore, behavior and activity level, fur condition, urination, defecation, feeding and water intake, surgical wound appearance was observed.

Peripheral blood samples and urine samples were collected at postoperative weeks 1, 2, 4, 8, and 12 for hematological and urinalysis assessments. Blood samples were analyzed using an automated veterinary hematology analyzer (Exigo eos, Sweden). The following parameters were recorded: WBC count and differential (granulocytes, lymphocytes, monocytes), RBC count, HGB concentration, PLT count.

Urine samples were analyzed using standard dipstick-based urinalysis PocketChem UA PU 4010 instrument to assess for signs of infection, hematuria, or inflammation.

4.7. Retrograde urethrography

To assess urethral patency and structure, retrograde urethrograms were performed at 4 and 12 weeks post-implantation. Rabbits were anesthetized as previously described. After disinfecting the surgical area with Octisept (0.1% octenidine dihydrochloride and 2% phenoxyethanol), the penis was gently extended caudally. An 8Ch catheter was inserted distal to the surgical site and secured with Vicryl 2/0 suture. A contrast agent solution (25% Urografin®, Bayer B.V.; sodium amidotrizoate/amidotrizoate meglumine) was injected through the catheter (10–20 ml), and radiographic images were obtained using a digital Medical ECONET mex + 100 x-ray machine (50 kV, 2.0 sec mAs^{-1}, 100 mA).

4.8. Histological analysis

At 12 weeks post-implantation, all animals were euthanized through intravenous overdose of a barbiturate anesthetic (Pentobarbital sodium). Under intramuscular sedation injecting of ketamine hydrochloride (35 mg kg^{-1}, Bioketan, Vetoquinol) and xylazine (5 mg kg^{-1}, Xylamed™, Bimeda), the 200 mg kg^{-1} dose of pentobarbital sodium (DOLETHAL 20% 250 ml (Vetoquinol) was performed ensuring successful calm and stressless euthanasia.

The entire penile structure, including the urethral graft region, was excised by transection at the penile root. Tissue specimens were fixed in 10% neutral buffered formalin for 24–36 h at RT. Samples were then processed through standard dehydration and paraffin embedding protocols. Paraffin blocks were sectioned transversely at 5 μm thickness using a HistoCore MULTICUT—Semi-Automated Rotary Microtome. Cross-sections were collected every 6 mm along the length of the graft region and mounted on Klinipath microscope KP frost printer slides. Histological staining was performed with: hematoxylin and eosin (H&E) for evaluation of tissue structure and cellularity. Staining protocol included standard deparaffinization and rehydration steps: deparaffinization: xylene baths (2 min × 2 repetitions); rehydration: graded ethanol series (99.7% isopropyl alcohol 2 min × 2 repetitions, and 96% ethyl alcohol 2 min × 2 repetitions); staining; washing steps; mounting: using Leica HistoCore SPECTRA CV X1, Mounting Medium. Histological evaluation was performed using Olympus BX40 microscope with 2×, 10×, 20× and 40× objectives for detailed cellular and structural assessment. Digital images were acquired using Aperio AT2 Digital Pathology Scanner and ImageScope x64 program. All tissue sections were evaluated in a blinded fashion by a single experienced pathologist. Histological findings were evaluated using a semiquantitative 0–2 scoring system, where 0 indicated healthy or unaffected tissue, 1 indicated mild pathological alteration, and 2 indicated the most severe or most pronounced pathological finding. Fibrosis was scored according to the degree of additional fibrous tissue formation in the subepithelial tissue: 0 indicated absence of additional fibrous tissue, 1 indicated mild fibrosis, and 2 indicated moderate to abundant fibrosis. Tissue inflammation was scored according to the degree of inflammatory cell infiltration, including lymphocytes, plasma cells, and neutrophils, in the subepithelial tissue: 0 indicated absence of inflammatory cell infiltration, 1 indicated mild infiltration, and 2 indicated moderate to abundant infiltration. Luminal inflammation was scored according to the degree of inflammatory cell infiltration, including lymphocytes, plasma cells, and neutrophils, within the urethral lumen: 0 indicated absence of inflammatory cells, 1 indicated mild infiltration, and 2 indicated moderate to abundant infiltration. Urothelial pathology was scored according to urothelial continuity, architecture, and cytological alteration: 0 indicated healthy urothelium without evident pathology, 1 indicated mild urothelial alteration, and 2 indicated severe urothelial damage, loss of continuity, or desquamation. Squamous epithelium was scored according to the extent of urothelial replacement by squamous epithelium: 0 indicated absence of squamous epithelial replacement,

1 indicated focal squamous metaplasia, and 2 indicated extensive or complete replacement of the urothelium by squamous epithelium. Hydrogel retention was scored according to the amount of hydrogel present in the subepithelial tissue: 0 indicated absence of hydrogel, 1 indicated minimal hydrogel retention, and 2 indicated moderate to abundant hydrogel retention.

4.9. Statistical analysis

Statistical analysis was performed using RStudio (version 4.3.3; R Foundation for Statistical Computing). Based on the small sample sizes, data were assumed to be normally distributed, and parametric methods were applied accordingly. One-way ANOVA was used to compare group differences at individual timepoints, and two-way ANOVA was employed for analyzing repeated measurements across multiple timepoints between groups. When significant effects were detected, estimated marginal means (EMMs) were calculated for pairwise post hoc comparisons using the rstatix package. Ordinal data (semiquantitative histological scoring) were analyzed using nonparametric tests, specifically the Kruskal–Wallis test, followed by Dunn's post hoc test for multiple comparisons. A p-value < 0.05 was considered statistically significant for all analyses. All animals enrolled in the study were included in the final analysis; no animals were excluded at any stage.

Acknowledgments

We would like to thank researchers of Vilnius University Laser Research Center for performing the SEM imaging. This project received funding from the European Regional Development Fund (Project No. 01.2.2-LMT-K-718-03-0087) under a Grant Agreement with the Research Council of Lithuania (LMT).

Data availability statement

All data that support the findings of this study are included within the article (and any supplementary files).

Supplementary material available at: https://doi.org/10.1088/1758-5090/ae9400/data1.

Conflict of interest

The authors declare no competing interests.

Author contributions

Aivaras Grybas 0009-0009-1890-452X
Conceptualization (equal), Data curation (equal), Investigation (equal), Methodology (equal), Writing – original draft (equal), Writing – review & editing (equal)

Povilas Barasa
Conceptualization (equal), Data curation (equal), Formal analysis (equal), Investigation (equal), Methodology (equal), Resources (equal), Writing – original draft (equal), Writing – review & editing (equal)

Darius Dasevicius
Data curation (equal), Formal analysis (equal), Visualization (equal)

Andrius Buivydas
Data curation (equal)

Ramune Tamasauske Zilinskaite 0000-0003-2205-2533
Conceptualization (equal), Investigation (equal), Methodology (equal), Writing – review & editing (equal)

Emilija Baltrukonyte
Data curation (equal), Investigation (equal)

Ieva Simoliune
Data curation (equal), Investigation (equal), Visualization (equal), Writing – review & editing (equal)

Milda Alksne
Investigation (equal), Writing – original draft (equal), Writing – review & editing (equal)

Natalija Krestnikova
Investigation (equal)

Arunas Zelvys
Conceptualization (equal), Funding acquisition (equal), Writing – review & editing (equal)

Daiva Baltriukiene
Conceptualization (equal), Funding acquisition (equal), Project administration (equal)

Gilvydas Verkauskas 0000-0001-7152-0802
Conceptualization (equal), Funding acquisition (equal), Methodology (equal), Project administration (equal), Resources (equal), Supervision (equal)

Feliksas Jankevicius
Conceptualization (equal), Writing – review & editing (equal)

Egidijus Simoliunas 0000-0001-5440-3591
Conceptualization (equal), Data curation (equal), Formal analysis (equal), Funding acquisition (equal), Investigation (equal), Methodology (equal), Supervision (equal), Visualization (equal), Writing – original draft (equal), Writing – review & editing (equal)

References

[1] Mundy A R 2006 Management of urethral strictures *Postgrad. Med. J.* **82** 489–93
[2] King C and Rourke K 2020 Re: urethral stricture is frequently a morbid condition: incidence and factors associated with complications related to urethral stricture *J. Urol.* **203** 655
[3] Yu X *et al* 2019 Hypospadias prevalence and trends in international birth defect surveillance systems, 1980–2010 *Eur. Urol.* **76** 482–90
[4] Van Der Horst H J R and De Wall L L 2017 Hypospadias, all there is to know *Eur. J. Pediatr.* **176** 435–41
[5] Cannoletta D, Pederzoli F, Yepes C, Joshi P, Salonia A, Briganti A, Montorsi F, Kulkarni S and Bandini M 2025 Evolution and innovation in urethroplasty: a comprehensive narrative review of graft types and surgical techniques *Int. J. Impot. Res.* **38** 38269–275
[6] Alsagheer G A, Fathi A, Abdel-kader M S, Hasan A M, Mohamed O, Mahmoud O and Abolyosr A 2018 Management of long segment anterior urethral stricture (⩾ 8cm) using buccal mucosal (BM) graft and penile skin (PS) flap: outcome and predictors of failure *Int. Braz. J. Urol.* **44** 163–71
[7] Hammouda H M, Shahat A A, Safwat A S and Taha T M 2024 The long-term consequences of the hypospadias salvage repair issue *BMC Pediatr.* **24** 58
[8] Dubey D, Vijjan V, Kapoor R, Srivastava A, Mandhani A, Kumar A and Ansari M S 2007 Dorsal onlay buccal mucosa versus penile skin flap urethroplasty for anterior urethral strictures: results from a randomized prospective trial *J. Urol.* **178** 2466–9
[9] Jin Y, Yang M, Zhao W, Liu M, Fang W, Wang Y, Gao G, Wang Y and Fu Q 2025 Scaffold-based tissue engineering strategies for urethral repair and reconstruction *Biofabrication* **17** 012003
[10] Mangir N, Wilson K J, Osman N I and Chapple C R 2019 Current state of urethral tissue engineering *Curr. Opin. Urol.* **29** 385–93
[11] El Kassaby A, AbouShwareb T and Atala A 2008 Randomized comparative study between buccal mucosal and acellular bladder matrix grafts in complex anterior urethral strictures *J. Urol.* **179** 1432–6
[12] Palminteri E, Berdondini E, Fusco F, De Nunzio C and Salonia A 2012 Long-term results of small intestinal submucosa graft in bulbar urethral reconstruction *Urology* **79** 695–701
[13] Campos-Juanatey F *et al* 2021 European association of urology guidelines on urethral stricture disease (part 2): diagnosis, perioperative management, and follow-up in males *Eur. Urol.* **80** 201–12
[14] Ortac M, Ekerhult T O, Zhao W and Atala A 2023 Tissue engineering graft for urethral reconstruction: is it ready for clinical application? *Urol. Res. Pract.* **49** 11–18
[15] Baghaei H, Faegh A, Jahani S, Hekmati P and Majidi Zolbin M 2025 Stem cell therapy for urethra and ureter tissue engineering: a systematic literature review on animal studies *Regen. Ther.* **30** 92–99
[16] Jin Y, Zhao W, Yang M, Fang W, Gao G, Wang Y and Fu Q 2023 Cell-based therapy for urethral regeneration: a narrative review and future perspectives *Biomedicines* **11** 2366
[17] Leibacher J and Henschler R 2016 Biodistribution, migration and homing of systemically applied mesenchymal stem/stromal cells mesenchymal stem/stromal cells—an update *Stem Cell Res. Ther.* **7** 7
[18] Park S-J, Kim H-J, Kim W, Kim O-S, Lee S, Han S-Y, Jeong E J, Park H-S, Kim H-W and Moon K-S 2016 Tumorigenicity evaluation of umbilical cord blood-derived mesenchymal stem cells *Toxicol. Res.* **32** 251–8
[19] Chapple C 2019 Tissue engineering of the urethra: where are we in 2019? *World J. Urol.* **38** 1–5
[20] Mandrycky C, Wang Z, Kim K and Kim D H 2016 3D bioprinting for engineering complex tissues *Biotechnol. Adv.* **34** 422–34
[21] Daly A C, Prendergast M E, Hughes A J and Burdick J A 2021 Bioprinting for the biologist *Cell* **184** 18–32
[22] Luraghi A, Peri F and Moroni L 2021 Electrospinning for drug delivery applications: a review *J. Control. Release* **334** 463–84
[23] Li K, Ding K, Zhu Q, Han F, He X, Tan S, Wu Z, Zheng Z, Tang Z and Liu Y 2023 Extracellular matrix stiffness aggravates urethral stricture through Igfbp3/Smad pathway *Sci. Rep.* **13** 14315
[24] Mak M S, Tsu J H and Lam W 2020 Endoluminal and endoscopic management of urethral stricture *J. Endoluminal. Endourol.* **3** e9–e18
[25] Hernández-hernández D, Ortega-gonzález M Y, Padilla-fernández B, Díaz-gonzález I, Climent-gonzález J and Hess-medler S 2025 Direct vision internal urethrotomy in the management of bulbar urethral strictures: long-term follow-up and factors predicting treatment failure *Urol. Int.* **109** 109560–565
[26] Vasudeva P, Nanda B, Kumar A, Kumar N, Singh H and Kumar R 2015 Dorsal versus ventral onlay buccal mucosal graft urethroplasty for long-segment bulbar urethral stricture: a prospective randomized study *Int. J. Urol.* **22** 967–71
[27] Lumen N *et al* 2021 European association of urology guidelines on urethral stricture disease (Part 1): management of male urethral stricture disease *Eur. Urol.* **80** 190–200
[28] Benson C R, Li G and Brandes S B 2021 Long term outcomes of one-stage augmentation anterior urethroplasty: a systematic review and meta-analysis *Int. Braz. J. Urol.* **47** 237–50
[29] Lumen N, Vierstraete-verlinde S, Oosterlinck W, Hoebeke P, Palminteri E, Goes C, Maes H and Spinoit A-F 2016 Buccal versus lingual mucosa graft in anterior urethroplasty: a prospective comparison of surgical outcome and donor site morbidity *J. Urol.* **195** 112–7
[30] Pal D, Gupta D, Ghosh B and Bera M 2016 A comparative study of lingual mucosal graft urethroplasty with buccal mucosal graft urethroplasty in urethral stricture disease: an institutional experience *Urol. Ann.* **8** 157
[31] Sharma G, Sharma S and Parmar K 2020 Buccal mucosa or penile skin for substitution urethroplasty: a systematic review and meta-analysis *Indian J. Urol.* **36** 81
[32] Hillary C J, Osman N I and Chapple C R 2014 Current trends in urethral stricture management *Asian J. Urol.* **1** 46–54
[33] Belsante M J *et al* 2015 The contemporary management of urethral strictures in men resulting from lichen sclerosus *Transl. Androl. Urol.* **4** 22–28
[34] Watanabe Y, Sasaki R, Matsumine H, Yamato M and Okano T 2017 Undifferentiated and differentiated adipose-derived stem cells improve nerve regeneration in a rat model of facial nerve defect: improvement of facial nerve regeneration by transplantation of adipose-derived stem cell *J. Tissue Eng. Regen. Med.* **11** 362–74
[35] Luo J, Zhao S, Wang J, Luo L, Li E, Zhu Z, Liu Y, Kang R and Zhao Z 2018 Bone marrow mesenchymal stem cells reduce ureteral stricture formation in a rat model via the paracrine effect of extracellular vesicles *J. Cell. Mol. Med.* **22** 4449–59
[36] Al-ghadban S and Bunnell B A 2020 Adipose tissue-derived stem cells: immunomodulatory effects and therapeutic potential *Physiol.* **35** 125–33

[37] Choi Y J, Kim W R, Kim D H, Kim J H and Yoo J H 2024 Human umbilical cord/placenta mesenchymal stem cell conditioned medium attenuates intestinal fibrosis *in vivo* and *in vitro Stem Cell Res. Ther.* **15**
[38] Wang Y, Ma M, Wang J, Zhang W, Lu W, Gao Y, Zhang B and Guo Y 2018 Development of a photo-crosslinking, biodegradable GelMA/PEGDA hydrogel for guided bone regeneration materials *Mater.* **11** 1345
[39] Xuan Z, Zachar V and Pennisi C P 2022 Sources, selection, and microenvironmental preconditioning of cells for urethral tissue engineering *Int. J. Mol. Sci.* **23** 14074
[40] Wong S S, Aboumarzouk O M, Narahari R, O'riordan A and Pickard R 2012 Simple urethral dilatation, endoscopic urethrotomy, and urethroplasty for urethral stricture disease in adult men *Cochrane Database Syst. Rev.* (https://doi.org/10.1002/14651858.CD006934.pub3)
[41] Li H, Xu Y, Fu Q and Li C 2012 Effects of multiple agents on epithelial differentiation of rabbit adipose-derived stem cells in 3D culture *Tissue Eng. A* **18** 1760–70
[42] Katz A J, Llull R, Hedrick M H and Futrell J W 1999 Emerging approaches to the tissue engineering of fat *Clin. Plast. Surg.* **26** 587–603
[43] Castiglione F *et al* 2016 Adipose-derived stem cells counteract urethral stricture formation in rats *Eur. Urol.* **70** 1032–41
[44] Xiao W *et al* 2016 Cell-laden interpenetrating network hydrogels formed from methacrylated gelatin and silk fibroin via a combination of sonication and photocrosslinking approaches *Mater. Sci. Eng. C* **99** 57–67
[45] Hussain M *et al* 2024 A review on PLA-based biodegradable materials for biomedical applications *Giant* **18** 100261
[46] Ntrivala M A *et al* 2025 Polycaprolactone (PCL): the biodegradable polyester shaping the future of materials—a review on synthesis, properties, biodegradation, applications and future perspectives *Eur. Polym. J.* **234** 114033
[47] Herrero-herrero M, Gómez-tejedor J A and Vallés-lluch A 2018 PLA/PCL electrospun membranes of tailored fibres diameter as drug delivery systems *Eur. Polym. J.* **99** 445–55
[48] Siegel A and Walton R M 2020 Hematology and biochemistry of small mammals In *Ferrets, Rabbits, and Rodents* pp 569–82 (Elsevier)
[49] Hendawy H, Farag A, Elhaieg A, Metwllay E, Shimada K, Elfadadny A and Tanaka R 2025 Enhanced bladder regeneration with adipose-derived stem cell-seeded silk fibroin scaffolds: a comparative analysis *Biomimetics* **10**
[50] Preda M B, Neculachi C A, Fenyo I M, Vacaru A-M, Publik M A, Simionescu M and Burlacu A 2021 Short lifespan of syngeneic transplanted MSC is a consequence of *in vivo* apoptosis and immune cell recruitment in mice *Cell Death Dis.* **12** 566
[51] Capuani S, Malgir G, Chua C Y X and Grattoni A 2022 Advanced strategies to thwart foreign body response to implantable devices *Bioeng. Transl. Med.* **7** e10300
[52] Jia L, Zhang P, Ci Z, Zhang W, Liu Y, Jiang H and Zhou G 2021 Immune-inflammatory responses of an acellular cartilage matrix biomimetic scaffold in a xenotransplantation goat model for cartilage tissue engineering *Front. Bioeng. Biotechnol.* **9** 667161
[53] Kyriakides T R, Kim H-J, Zheng C, Harkins L, Tao W and Deschenes E 2022 Foreign body response to synthetic polymer biomaterials and the role of adaptive immunity *Biomed. Mater.* **17** 022007
[54] Van Niekerk G and Engelbrecht A-M 2018 Inflammation-induced metabolic derangements or adaptation: an immunometabolic perspective *Cytokine Growth Factor Rev.* **43** 47–53
[55] Liu Y-X, Sun J-M, Ho C-K, Gao Y, Wen D-S, Liu Y-D, Huang L and Zhang Y-F 2023 Advancements in adipose-derived stem cell therapy for skin fibrosis *World J. Stem Cells* **15** 342–53
[56] Vanderstichele S and Vranckx J J 2022 Anti-fibrotic effect of adipose-derived stem cells on fibrotic scars *World J. Stem Cells* **14** 200–13
[57] Jackson J, Samarah H, Palmer W, Kaplan Z, Nicodem M, Kumar P, Short S, Bridgham K, Harshyne L and Curry J 2025 The impact of biomaterial characteristics on macrophage phenotypes in tissue engineering: a review *Plast. Aesthetic Res.* (https://doi.org/10.20517/2347-9264.2024.166)
[58] Ten Brink T, Damanik F, Rotmans J I and Moroni L 2024 Unraveling and harnessing the immune response at the cell–biomaterial interface for tissue engineering purposes *Adv. Healthc. Mater.* **13** 2301939
[59] Chung Y G, Algarrahi K, Franck D, Tu D D, Adam R M, Kaplan D L, Estrada C R and Mauney J R 2014 The use of bi-layer silk fibroin scaffolds and small intestinal submucosa matrices to support bladder tissue regeneration in a rat model of spinal cord injury *Biomaterials* **35** 7452–9
[60] Kuniakova M *et al* 2023 Decellularization of the human urethra for tissue engineering applications *Exp. Biol. Med.* **248** 1034–42
[61] Wang B, Lv X, Li Z, Zhang M, Yao J, Sheng N, Lu M, Wang H and Chen S 2020 Urethra-inspired biomimetic scaffold: a therapeutic strategy to promote angiogenesis for urethral regeneration in a rabbit model *Acta Biomater.* **102** 247–58
[62] Algarrahi K, Affas S, Sack B S, Yang X, Costa K, Seager C, Estrada C R and Mauney J R 2018 Repair of injured urethras with silk fibroin scaffolds in a rabbit model of onlay urethroplasty *J. Surg. Res.* **229** 192–9
[63] Lv X, Feng C, Liu Y, Peng X, Chen S, Xiao D, Wang H, Li Z, Xu Y and Lu M 2018 A smart bilayered scaffold supporting keratinocytes and muscle cells in micro/nano-scale for urethral reconstruction *Theranostics* **8** 3153–63
[64] Tian B, Song L, Liang T, Li Z, Ye X, Fu Q and Li Y 2018 Repair of urethral defects by an adipose mesenchymal stem cell-porous silk fibroin material *Mol. Med. Rep.* (https://doi.org/10.3892/mmr.2018.9001)
[65] Wang C, Chen C, Guo M, Li B, Han F and Chen W 2019 Stretchable collagen-coated polyurethane-urea hydrogel seeded with bladder smooth muscle cells for urethral defect repair in a rabbit model *J. Mater. Sci. Mater. Med.* **30** 135
[66] Jiao W, Yu W, Wang Y, Zhang J, Wang Y, He H and Shi G 2023 Fibrinogen/poly(l-lactide-co-caprolactone) copolymer scaffold: a potent adhesive material for urethral tissue regeneration in urethral injury treatment *Regen. Ther.* **22** 136–47
[67] Abbas T O, Parangusan H, Yalcin H C, Hassan M, Zakrif L, Zandi N and Pennisi C P 2024 Trilayer composite scaffold for urethral reconstruction: *in vitro* evaluation of mechanical, biological, and angiogenic properties *Biomed. Mater.* **19** 025022
[68] Cunnane E M, Davis N F, Cunnane C V, Lorentz K L, Ryan A J, Hess J, Weinbaum J S, Walsh M T, O'brien F J and Vorp D A 2021 Mechanical, compositional and morphological characterisation of the human male urethra for the development of a biomimetic tissue engineered urethral scaffold *Biomaterials* **269** 120651
[69] Orabi H, Bouhout S, Morissette A, Rousseau A, Chabaud S and Bolduc S 2013 Tissue engineering of urinary bladder and urethra: advances from bench to patients *Sci. World J.* **2013** 154564
[70] Abbas T O, Yalcin H C and Pennisi C P 2019 From acellular matrices to smart polymers: degradable scaffolds that are transforming the shape of urethral tissue engineering *Int. J. Mol. Sci.* **20** 1763
[71] Zamani M, Shakhssalim N, Ramakrishna S and Naji M 2020 Electrospinning: application and prospects for urologic tissue engineering *Front. Bioeng. Biotechnol.* **8** 579925
[72] Sack B S, Mauney J R and Estrada C R 2016 silk fibroin scaffolds for urologic tissue engineering *Curr. Urol. Rep.* **17**
[73] An Z *et al* 2025 The BAM-GelMA ADSCs bilayer patch promotes tissue regeneration and functional recovery after large-area bladder defects in beagles *Bioeng. Transl. Med.* **10** e10745
[74] Hua Y *et al* 2023 Four-dimensional hydrogel dressing adaptable to the urethral microenvironment for scarless urethral reconstruction *Nat. Commun.* **14** 7632

[75] Liu Y et al 2017 Urethral reconstruction with autologous urine-derived stem cells seeded in three-dimensional porous small intestinal submucosa in a rabbit model *Stem Cell Res. Ther.* **8** 63
[76] Wan X, Yao H, Wei Z, Gao D, Zheng D, Xu B and Xie M 2025 Heterogeneous porous hypoxia-mimicking scaffolds propel urethral reconstruction by promoting angiogenesis and regulating inflammation *Biomaterials* **314** 122833
[77] Wu S, Liu Y, Bharadwaj S, Atala A and Zhang Y 2011 Human urine-derived stem cells seeded in a modified 3D porous small intestinal submucosa scaffold for urethral tissue engineering *Biomaterials* **32** 1317–26
[78] Chang M, Tan Q, Bian G, Zhang M, Lv J, Su J and Wang X 2025 A double-layer PLGA/CoI-MeHA tissue engineering scaffold for urethral reconstruction *Front. Pharmacol.* **16** 1555183
[79] Orabi H, Aboushwareb T, Zhang Y, Yoo J J and Atala A 2013 Cell-seeded tubularized scaffolds for reconstruction of long urethral defects: a preclinical study *Eur. Urol.* 63531–538
[80] Grayson W L, Bhumiratana S, Grace Chao P H, Hung C T and Vunjak-novakovic G 2010 Spatial regulation of human mesenchymal stem cell differentiation in engineered osteochondral constructs: effects of pre-differentiation, soluble factors and medium perfusion *Osteoarthr. Cartil.* **18** 714–23
[81] Pranskunas M, Šimoliūnas E, Alksne M, Martin V, Gomes P S, Puisys A, Kaupinis A and Juodzbalys G 2021 Assessment of the bone healing process mediated by periosteum-derived mesenchymal stem cells' secretome and a xenogenic bioceramic—an *In Vivo* study in the rabbit critical size calvarial defect model *Mater.* **14** 3512
[82] Barasa P et al 2023 Differentiation of rabbit stem cells on gelatin for tissue engineering applications*IFMBE Proc.* (Springer Science and Business Media Deutschland GmbH) vol 89 pp 278–86
[83] Versteegden L R M, de Jonge Paul K J D, IntHout J, van Kuppevelt T H, Oosterwijk E, Feitz Wout F J, de Vries Rob B M and Daamen W F 2017 Tissue engineering of the urethra: a systematic review and meta-analysis of preclinical and clinical studies [Figure presented] *Eur. Urol.* **72** 594–606